Editors' Suggestion

Pressure-induced charge-transfer and structural transition in hexagonal multiferroic $HoMnO_3$

Martin Ottesen,[1] Emma Ehrenreich-Petersen,[1] Camilla Hjort Kronbo,[1] François Baudelet,[2] Lucie Nataf,[2] Innokenty Kantor,[3] Mads Ry Vogel Jørgensen,[1,3] and Martin Bremholm[1,*]

[1]*Department of Chemistry and iNANO, Aarhus University, Langelandsgade 140, 8000 Aarhus C, Denmark*
[2]*Synchrotron SOLEIL, L'Orme des Merisiers, Saint-Aubin, BP48, 91192 Gif-sur-Yvette, France*
[3]*MAX IV Laboratory, Lund University, Fotongatan 2, SE-221 00 Lund, Sweden*

(Received 25 January 2023; accepted 6 April 2023; published 25 April 2023)

The structural properties of the hexagonal multiferroic h-$HoMnO_3$ under high pressure have been explored using synchrotron x-ray diffraction and x-ray absorption spectroscopy in diamond anvil cells. The structure was found to undergo a pressure-induced phase transition at ∼24 GPa to a rhombohedrally distorted superstructure, which is isostructural to the oxygen-loaded h-$RMnO_{3+\delta}$ (R = Y, Dy, Ho, Er; $\delta \approx 0.28$) phases found in the same systems. The driving force behind the phase transition is the highly compressible *ab* plane which facilitates a gradual charge disproportionation of Mn(III) with pressure. We speculate this stabilizes the spin-liquid phase due to ferromagnetic coupling between neighboring Mn(II)/Mn(IV) and Mn(III). In addition, we demonstrate that the structural behavior is highly susceptible to nonhydrostatic conditions and the choice of pressure medium should be carefully made.

DOI: 10.1103/PhysRevB.107.134115

I. INTRODUCTION

The rare-earth manganites, $RMnO_3$ (R = La–Lu), host a wide range of novel structural and physical properties which are highly dependent on the choice of R. At ambient conditions the compounds with the larger rare-earth cations (R = La–Dy) adopt the orthorhombic $GdFeO_3$ perovskite structure type (o-$RMnO_3$, space group *Pnma*, No. 62), whereas for the smaller R cations (R = Ho–Lu, Y, In, Sc) the system crystallizes in a hexagonal structure (h-$RMnO_3$, space group $P6_3cm$, No. 185). While both polymorphs exhibit multiferroic behavior with the coexistence of antiferromagnetism and improper ferroelectricity [1–3], the underlying mechanism is vastly different. In o-$RMnO_3$, the inversion breaking required for ferroelectricity coincides with the appearance of spiral magnetic ordering, known as a type-II multiferroic, as observed in, e.g., o-$TbMnO_3$ at $T \sim 28$ K [4,5]. In h-$RMnO_3$, the onset of ferroelectric and antiferromagnetic ordering occurs at very different temperatures ($T_C \sim 1000$ K [6], $T_N \sim 80$–100 K [7]) and they are thus classified as type-I multiferroics. Here, the ferroelectric transition arises due to a structural phase transition from a nonpolar $P6_3/mmc$ to the polar $P6_3cm$ phase with $\vec{P} \parallel c$ [8,9]. The structure consists of alternating MnO and RO layers, both of which span a two-dimensional triangular sublattice. The MnO layer consists of corner-shared MnO_5 trigonal bipyramidal units and below the ferroelectric Curie temperature, the bipyramidal units trimerize due to tilting toward a bridging oxygen which is the source of its novel physical properties [2,10]. The structure and trimerization are shown in Fig. 1. In h-$HoMnO_3$, below $T_N \sim 75$ K, the Mn(III) moments align in the basal plane with an antiferromagnetic (AFM) coupling between nearest neighbors via superexchange interactions through the Mn-O-Mn bonds [11]. Due to the triangular sublattice this results in a highly frustrated geometry with a 120° angle between the spins. At T_N, dielectric anomalies have been reported in all hexagonal rare-earth manganites [12–15]. These interactions, which should normally be forbidden by symmetry, are mediated through the lattice by a giant magnetoelastic coupling manifesting spin-induced lattice strain owing to the intrinsically frustrated triangular lattice [16,17]. In addition, significant magnetic diffuse scattering well below T_N in h-$YMnO_3$ suggests the coexistence of the long-range AFM ordering with a short-range spin-liquid state [18] and isostructural $TbInO_3$ shows no evidence of long-range in-plane magnetic ordering of Tb(III) down to 0.15 K [19]. Whether these spin fluctuations are a result of a spin-liquid phase or arise due to critical scattering is still debated [20].

Despite the highly intricate interaction between the lattice and the exotic multiferroic properties displayed in these systems, few studies have explored the consequence of applying external pressure. From a structural perspective, evidence of a kinetically hindered phase transition from h-$RMnO_3$ to the perovskite o-$RMnO_3$ phase at 10–20 GPa has previously been reported [21–24]; however, conflicting data showing no

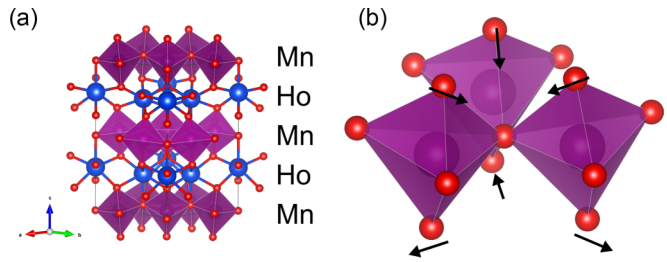

FIG. 1. (a) Crystal structure of h-$HoMnO_3$ consisting of alternating MnO and HoO layers. Mn, Ho, and O atoms are displayed in pink, blue, and red, respectively. (b) Three corner-shared MnO_5 bipyramids tilt toward a bridging oxygen forming a trimer unit.

*Corresponding author: bremholm@chem.au.dk

structural transitions have also been reported [25]. Stabilizing the orthorhombic polymorph for the smaller R can be done with a combination of high pressure and high temperature [26–28], but pressure alone seems unlikely due to the fundamentally different structural motif. To help clarify the discrepancies regarding the high-pressure behavior, we have performed synchrotron high-pressure powder x-ray diffraction (PXRD) on h-$HoMnO_3$ from 0–40 GPa. We report the discovery of a high-pressure structural phase transition of h-$HoMnO_3$ to a rhombohedral distorted superstructure with space group $R3c$ and demonstrate the sensitivity of these structures to nonhydrostatic conditions. In addition, we demonstrate that this phase transition is accompanied with a gradual charge disproportionation of Mn(III) to Mn(II) and Mn(IV) by tracking changes to the Mn K edge using high-pressure x-ray absorption near edge structure (HP-XANES) and discuss its implications on the magnetic ordering with pressure.

II. METHODS

A. Synthesis

Powder samples of hexagonal h-$HoMnO_3$ were prepared using a standard solid-state synthesis route. Due to the hygroscopicity of the rare-earth sesquioxide, Ho_2O_3 was heated to 950 °C for 16 h and then thoroughly mixed with stoichiometric amounts of Mn_2O_3 in an agate mortar. The mixture was pressed into pellets and calcined twice at 1250 °C for 24 h with intermediate grinding. Sample purity was confirmed using PXRD measured with a Rigaku SmartLab diffractometer (Cu Kα_1, $\lambda = 1.5406$ Å).

B. High-pressure PXRD

High-pressure PXRD measurements were performed at the Advanced Photon Source (APS) GSECARS [29] beamline BM-13-D ($\lambda = 0.3344$ Å, beam size $\sim 5 \times 8$ μm^2). Samples were ground to very fine powders and subsequently floated in ethanol to segregate particles by size. The isolated microscopic crystallites were pressed together between two opposing diamond anvils to obtain highly dense sample pieces with size of approximately $20 \times 30 \times 10$ μm^3. Samples were loaded in Mao-Bell type symmetric diamond anvil cells, with culet size of 200 μm, along with a small piece of gold for pressure calibration and a ruby sphere which was used during gas loading at GSECARS [30]. A 250 μm thick rhenium gasket was indented to 35 μm and a hole of 100 μm was laser drilled which served as the sample chamber. Neon was used as the pressure-transmitting medium and was gas-loaded into the sample chamber.

An additional run with silicone oil as the pressure medium was performed at the DanMAX beamline, MAX IV ($\lambda = 0.3757$ Å, beam size $\sim 21 \times 9$ μm^2). Here, copper was used as the pressure calibrant and a 90 μm sample chamber was drilled using electrical discharge machining (EDM) with the rest of the experimental procedure being identical to the experiment performed at APS.

Diffractograms at APS were recorded on a 2D image plate detector and the geometry was calibrated using CeO_2, and diffractograms at DanMAX were recorded on a Dectris Pilatus3 X 2M CdTe area detector calibrated with a Si standard. All 2D diffractograms were integrated using the Dioptas software [31] and subsequent Rietveld refinement was performed in the FullProf software suite [32]. The extracted unit cell volume was fitted with a third-order Birch-Murnaghan EoS model using the EoSFit-7 program [33]. Structure models were drawn using the VESTA software [34]. An ambient data set was recorded at APS, which served as the structural model for subsequent refinements of high-pressure diffractograms. The Rietveld refinement and the structural parameters are found in the Supplemental Material (SM) [35].

C. High-pressure XAS

The high-pressure XAS measurements were performed at the ODE beamline of synchrotron SOLEIL. This beamline is especially suitable for high-pressure experiments thanks to its dispersive setup giving a focus spot of $\sim 30 \times 30$ μm^2 FWHM and a fast acquisition [36]. High pressure was obtained through membrane diamond anvils cells, Le Toullec design with Re gasket, preindented to 20 μm thick and perforated with a 150 μm hole using EDM. The sample chamber was then filled with the floated powder, a ruby ball as pressure gauge, and gas-loaded with He as pressure-transmitting medium. The pressure was determined using the ruby photoluminescence technique [37]. Measurements were performed at the Mn K edge and at the Ho L_3 edge, using the Si 311 blade as polychromator, giving a resolution of 0.5 eV.

XAS data were processed and normalized using ATHENA from the Demeter software package [38].

III. RESULTS AND DISCUSSION

The PXRD pressure series of h-$HoMnO_3$ is plotted in Fig. 2. The system remains in its ambient configuration until a structural phase transition is observed at 24 GPa. Close inspection of the changes in the diffraction patterns reveals the transition is related to modulation of the hexagonal c axis. For instance, the (002) and (004) reflections develop a shoulder on the high-Q side accompanied with rapid decrease of the intensity in these reflections. On the other hand, the (110) reflection remain unchanged. Therefore, the appearance of the two new peaks on equidistant sides of the hexagonal (102) reflection suggests a superstructure along the hexagonal c axis. Comparison between the d spacing of the hexagonal (102) reflection with the two new peaks was consistent with a unit cell of the form $a' \approx a_H$ and $c' \approx 3c_H$. Analysis of systematic absences is consistent with a rhombohedral centering, suggesting the space group $R3c$ corresponding to a first-order phase transition. The two phases coexist in the pressure range 24–38 GPa, suggesting a rather sluggish transition common for first-order phase transitions. Interestingly, similar superlattice reflections have previously been reported in the hexagonal rare-earth manganite family related to their oxygen-storage properties as demonstrated in, e.g., $DyMnO_{3.25}$ [39], $HoMnO_{3.28}$ [40,41], and the solid solutions $Dy_{1-x}Y_xMnO_{3.25}$ [42] and $YMn_{1-x}Ti_xO_{3+\delta}$ [43–45]. In this phase, commonly referred to as Hex_1, the excess oxygen coordinates around the Mn atoms, promoting a partial oxidation of Mn(III) to Mn(IV). To gain further insight into the pressure-induced phase transition a Rietveld refinement was done at 40 GPa based on

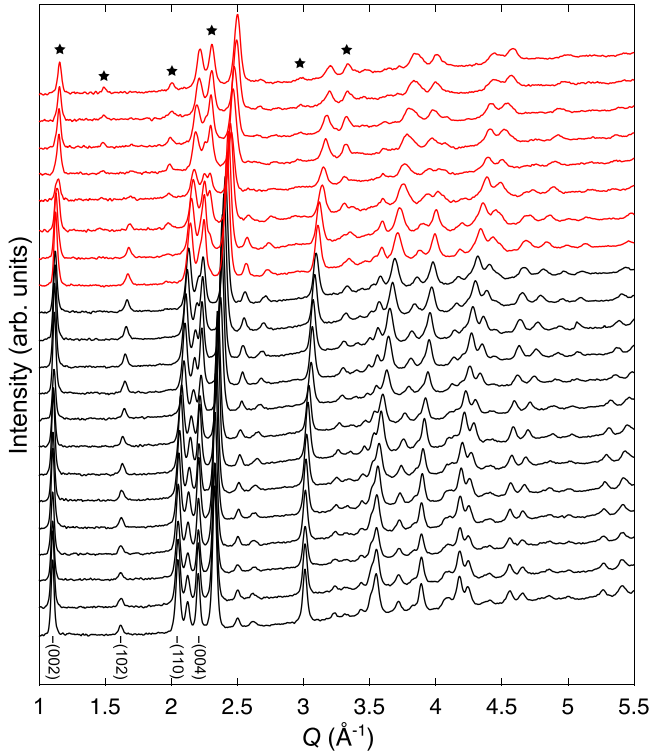

FIG. 2. HP-PXRD waterfall plot. A pressure-induced phase transition is observed with an onset pressure of 24 GPa (red diffractograms). Selected peaks indicating the appearance of a new phase are marked with a star. Miller indices are with respect to the ambient $P6_3cm$ structure.

the rhombohedral Hex_1 superstructure which can be seen in Fig. 3(a). The structural model provides an excellent description of the high-pressure phase, strongly suggesting a deeper connection between the oxygen-storage properties and the effect of hydrostatic pressure. Structural refinement parameters for the $R3c$ phase at 40 GPa can be found in the SM [35]. The structural motif of the rhombohedral superstructure is similar to the ambient structure with alternating layers of tilted MnO_5 trimers and HoO_7 polyhedra, but the elongated c axis stems from changes to the stacking of the MnO_5 layers. In the ambient $P6_3cm$ structure, alternating MnO_5 layers are related by a 60° rotation normal to the bridging oxygen in the trimer, as sketched in Fig. 3(b), resulting in an A-B-A-B type stacking. In the $R3c$ structure, adjacent layers are still rotated by 60° but with an additional translational shift with respect to the layers immediately above and below as seen in Fig. 3(c). The stacking sequence thus become a distorted A-B packing, with each A and B layer having a translational periodicity of three. The structure can thus be represented by a stacking sequence of $A_1{-}B_2{-}A_3{-}B_1{-}A_2{-}B_3{-}A_1{-}B_2{-}\cdots$, where subscripts 1, 2, and 3 correspond to the positions (0 0 z), (2/3 1/3 z), and (1/3 2/3 z) of the central oxygen [43]. Substituting Mn with Ti was shown to have a significant effect on the magnetic properties in $YMn_{1-x}Ti_xO_{3+\delta}$ [45]. Here it was demonstrated that the hexagonal to rhombohedral phase transition occurred for $x \geqslant 0.20$ and was accompanied by quenching of the magnetic ordering with increasing Ti content as the Weiss temperature approaches 0 across the phase transition. The

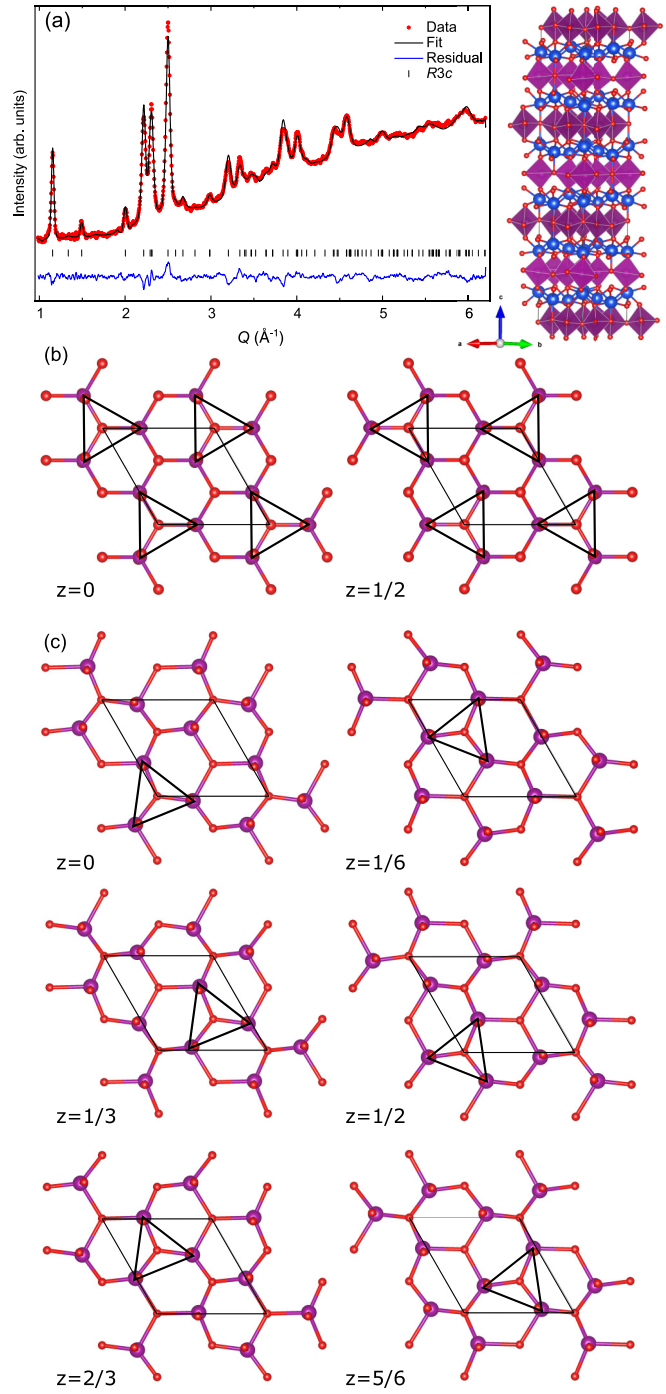

FIG. 3. (a) Rietveld refinement of the rhombohedral $R3c$ phase at 40 GPa. The structure corresponds to a distorted version of the ambient phase. (b) A-B stacking sequence of MnO_5 trimer units at $z = 0$ and $z = 1/2$ in the ambient $P6_3cm$ phase. The trimer orientations are shown with triangles around the bridging oxygen, O3. (c) Stacking sequence of MnO_5 trimers in the high-pressure $R3c$ phase showing the translational shift at each subsequent layer. The left column corresponds to the A layer while the right column corresponds to the B layer

disappearance of long-range antiferromagnetic ordering was likewise demonstrated using neutron powder diffraction for $x = 0.25$ [43]. Assuming stoichiometric oxygen composition, the authors argued the suppression of magnetic coupling

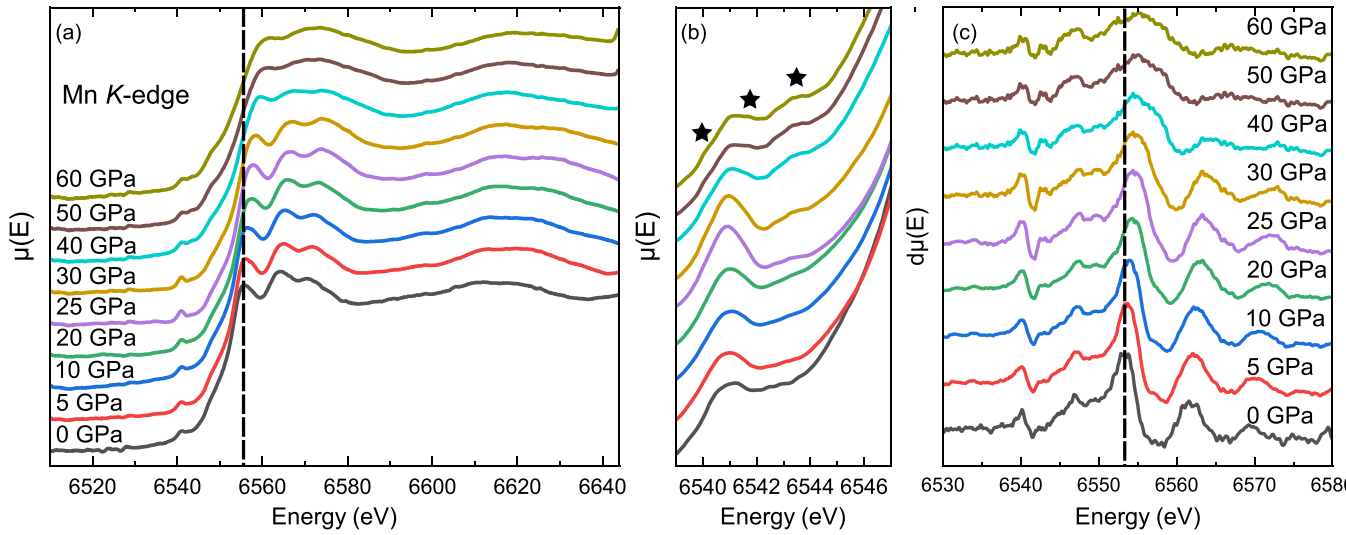

FIG. 4. (a) HP-XANES measurements on the Mn *K* edge. Mn undergoes a profound change with pressure with a gradual shift and broadening of the edge starting at 5 GPa. (b) The pre-edge region reveals two new features on either side of the $1s \rightarrow 3d$ transition peak at 6541 eV indicating the presence of Mn(II) and Mn(IV). The set of transitions near 6543 eV, marked by a star, increases in intensity with increasing pressure related to an increased local distortion and valence change of Mn. (c) First derivative of the Mn spectra which further highlights the observed changes. The dashed lines are a guide to the eye.

stems from the formation of Ti(IV) which introduces electrons into the Mn site, forming Mn(II) ions, consequently disrupting the magnetic properties. However, a combined gravimetric analysis and XAS study demonstrated that the introduction of Ti further promotes the partial oxidation of Mn(III) to Mn(IV), with facile absorption of atmospheric oxygen upon cooling [44]. Thus, if the high-pressure phase of hexagonal $HoMnO_3$ is indeed isostructural to the oxygen-loaded Hex_1 $RMnO_{3+\delta}$ phase, then it would suggest the transition is not a consequence of strain induced by chemical pressure upon introduction of excess oxygen, but rather directly linked to the formation of Mn(IV) ions in the structure. This suggests that the appearance of the rhombohedral Hex_1 phase is of possible magnetoelastic origin. Considering neon was used as pressure-transmitting medium in this work, the formation of Mn(IV) can only occur due to a charge disproportionation of the form $2\text{Mn(III)} \rightarrow \text{Mn(IV)} + \text{Mn(II)}$ or from a charge transfer between Ho and Mn. To verify this hypothesis, HP-XANES was performed on the Ho L_3 edge (see SM [35]) and the Mn *K* edge from 0–60 GPa as seen in Fig. 4. While there are no changes to the Ho L_3 edge, the Mn *K* edge undergoes significant alterations with increasing pressure. Even at 5 GPa there is a gradual shift of the main edge peak toward higher energies. The pre-edge is shown in Fig. 4(b). The feature at ~6541 eV corresponds to the $1s \rightarrow 3d$ transition. This peak develops two shoulders, one on either side, in good agreement with the formation of Mn(II) and Mn(IV) species [46]. The second set of pre-edge features, near 6543 eV, is observed in both Mn(III)- and Mn(IV)-based compounds but their intensity is sensitive to both oxidation state and the local distortion [46]. As seen, the intensity of these features increases sharply above the transition pressure, consistent with the distortion of the MnO_5 unit as observed with PXRD. To better visualize the pressure-dependent changes to the absorption edge, defined as the maxima in the first derivative with respect to energy, the derivative of the spectra in Fig. 4(a) is plotted in Fig. 4(c). The position of the edge shifts toward higher energies but is accompanied by significant broadening. This is consistent with the model of having gradual charge disproportionation of Mn(III), resulting in a mixture of Mn(II), Mn(III), and Mn(IV) ions in the structure. The rhombohedral structural model contains only one unique Mn position, while normally a charge disproportionation would result in symmetry-inequivalent atomic positions. However, no additional reflections are observed which could be assigned to a potential lower symmetry of the *ab* plane. In addition, the occurrence of charge disproportionation within the Mn trimer is therefore likely to suppress the long-range AFM coupling, trapping the structure in its spin-liquid state due to the geometric frustration from the hexagonal sublattice [18]. In turn, this is expected to have a profound effect on the magnetoelastic coupling, quenching the multiferroic properties with increasing pressure. Indeed, the suppression of the AFM state and gradual decrease of the magnetic moment at high pressure has been demonstrated in hexagonal $YMnO_3$ and $LuMnO_3$ using neutron powder diffraction [47,48] up to 6.7 GPa with the effect being more pronounced in the yttrium variant. This can be directly correlated to the oxidative properties of Mn in these materials which are exceedingly sensitive to the size of the rare-earth cation, *R* [40,42]. As the size of *R* decreases, the more difficult it becomes to load oxygen into the structure and, by extension, form Mn(IV). By changing *R* the tilting angle shows a systematic variation with larger tilt for smaller *R* which increases the nearest-neighbor superexchange interaction as seen by an increase of T_N through the series. This suggests a direct correlation between the oxygen-storage and multiferroic properties in the hexagonal family. Interestingly, a high-oxygen-content orthorhombic $Pca2_1$ phase has been reported in $RMnO_{3+\delta}$ with $\delta = 0.40$ for $R = \text{Y, Ho, Er}$ [40] but we have not observed this phase up to the highest measured pressure of 40 GPa.

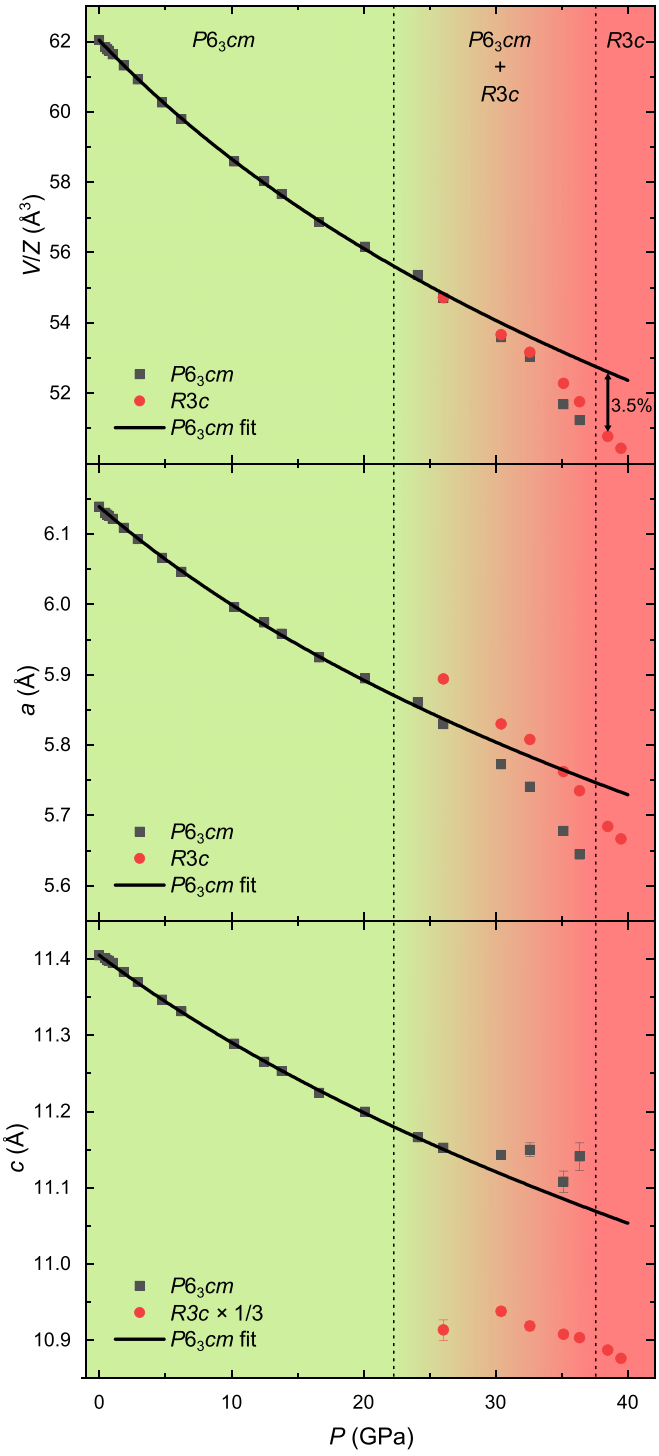

FIG. 5. Unit cell parameters as a function of pressure with the obtained equation of state fit. Fitting was done from 0–26 GPa on the hexagonal $P6_3cm$ phase corresponding to a refined weight fraction below 50%. The volume has been normalized with the number of formula units ($Z = 6$ for $P6_3cm$, $Z = 18$ for $R3c$), and the c axis of the rhombohedral phase has been scaled by 1/3 for comparison with the hexagonal phase. A volume collapse of 3.5% is estimated based on extrapolation of the fit at 38.5 GPa.

Unit cell parameters were extracted by Rietveld refinement and have been plotted as a function of pressure in Fig. 5 along with the fitted third-order Birch-Murnaghan (BM) isothermal equation of state (EoS):

$$P(V) = \frac{3K_0}{2}\left[\left(\frac{V_0}{V}\right)^{\frac{7}{3}} - \left(\frac{V_0}{V}\right)^{\frac{5}{3}}\right] \times\left\{1 + \frac{3}{4}(K_0' - 4)\left[\left(\frac{V_0}{V}\right)^{\frac{2}{3}} - 1\right]\right\}, \quad (1)$$

where P is the pressure, V_0 is the reference volume, K_0 is the ambient pressure bulk modulus, and K_0' is the pressure derivative of the bulk modulus. The same equation can be used to determine the ambient pressure linear modulus, M_0^i, along a principal axis, i. By cubing one of the lattice parameters, a volume-like fit using Eq. (1) with $V = i^3$ can be performed. From this it follows that $M_0^i = 3K_0$ and $M_0^{i\prime} = 3K_0'$ [33]. While the ambient phase persisted up to 38 GPa, the fit was done in the range of 0–26 GPa since the introduction of the rhombohedral phase causes significant instability with increasing weight fraction due to the large degree of peak overlap between the ambient and high-pressure phase. The extracted weight fraction of the high-pressure phase with pressure is given in the SM along with the fitted unit cell parameters for both phases [35]. From Eq. (1) the bulk modulus was found to be $K_0 = 157(4)$ GPa with $V_0 = 372.209(15)$ Å^3 and $K_0' = 4.8(4)$. The fitted parameters can also be found in Table I with comparison to pressure studies performed on other members of the hexagonal family. The covariance ellipsoids are shown in the SM [35]. The bulk moduli are comparable across the series, but with a tendency for higher bulk modulus for the smaller rare-earth cations of Tm and Lu, likely as a result of tuning the chemical pressure which may put additional strain on the structure. Substituting with smaller R results in a gradually higher c/a ratio, indicating the cell is more compressible in the ab plane. This modifies the Mn-O-Mn superexchange pathway in the triangular sublattice with increased tilting of the MnO_5 bipyramidal units [49] which results in the increasing T_N across the series [2]. Fitting the unit cell parameters with Eq. (1) we extract a linear modulus for the a axis of $M_0^a = 380(9)$ GPa with $a_0 = 6.13876(11)$ Å and $M_0^{a\prime} = 12.2(11)$, and for the c axis $M_0^c = 879(18)$ GPa with $c_0 = 11.40504(17)$ Å and $M_0^{c\prime} = 25(3)$. The compressibility of the a axis is more than twice the compressibility of the c axis which is expected to have a profound impact on the geometry of the MnO_5 trimer and as a consequence the magnetic properties under pressure. This surprising response is a common property found in both the hexagonal manganites (see Table I and references therein) and indites [52,53] alike. The unit cell ratio c/a of the hexagonal phase has been plotted as a function of pressure in Fig. 6. The c/a ratio smoothly increases with pressure in a nonlinear behavior likely contributing to a steadily increasing lattice strain. As the ab plane is compressed the hybridization between the Mn $3d$ states and in-plane oxygen $2p$ states increases which may provide the pathway necessary for charge disproportionation to occur. The formation of Mn(II) ions by Zr(IV)-doping into the R(III) site has previously been shown to suppress the AFM ordering and stabilize the spin-liquid state [49]. This suggests that the Mn(II)-Mn(III) interaction

TABLE I. Comparison of ionic radii, r, bulk modulus, K_0, its pressure derivative, K_0', the linear moduli of the a and c axes, M_0^a and M_0^c, type and pressure of the observed structural transition, and the ratio c_0/a_0 at ambient pressure for different R in h-RMnO$_3$. NOB = not observed.

R	r (Å)[a]	K_0 (GPa)	K_0'	M_0^a (GPa)	M_0^c (GPa)	Transition	c_0/a_0[b]
Y	0.96	157(5)[c], 112(8)[d]	12(2)[c], 12.3(14)[d]	667[3]	1429[3]	NOB (30 GPa)[3], *Pnma* (22 GPa)[d]	1.854
Ho	0.96	157(3)[e], 130(7)[d]	4.8(4)[e], 14.3(15)[d]	380(9)[e]	879(18)[e]	*R*3*c* (24 GPa)[e]	1.855
Er	0.95	163(14)[f]	4.5(15)[f]	–	–	*Pnma* (20 GPa)[f]	1.864
Tm	0.94	189(14)[g]	4[g]	–	–	*Pnma* (10 GPa)[g]	1.870
Lu	0.92	180(6)[c], 110(12)[d]	12(2)[c], 26(4)[d]	833[c]	1667[c]	NOB (30 GPa)[c], *Pnma* (22 GPa)[d]	1.881

[a]7-coordinated R(III) ionic radii from Ref. [50] and Ref. [51].
[b]Ambient unit cell parameters taken from Ref. [28] for internal consistency.
[c]From Jabarov *et al.* [25], fit with 3rd-order BM, 15:3:1 methanol-ethanol-water.
[d]From Gao *et al.* [23], fit with 1st-order Murnaghan, 15:3:1 methanol-ethanol-water.
[e]This work, neon.
[f]From Lin *et al.* (Ref. [24]), fit with 3rd-order BM, silicone oil.
[g]From Wang *et al.* (Ref. [22]), fit with 2nd-order BM ($K_0' = 4$ fixed), 4:1 methanol-ethanol.

is ferromagnetic. Since the same tendency has been found in the oxygen-loaded systems, the Mn(IV)-Mn(III) interaction is likely ferromagnetic as well. These findings explain the extreme sensitivity of the AFM state to pressure, as demonstrated in h-YMnO$_3$ and h-LuMnO$_3$ [47,48], by means of a pressure-dependent Mn(III)-Mn(III) charge disproportionation which can be correlated to the size of R, and in turn, their oxygen-storage properties. The magnetic behavior of h-HoMnO$_3$ is special compared to the other rare-earth manganites since it undergoes a spin rotation at $T_{SR} \sim 33$ K [11] where the transition temperature has been shown to be highly sensitive to applied external pressure [16]. The large compressibility of the *ab* plane is consistent with the structural model of the rhombohedral HP phase being a distorted version of the ambient hexagonal phase. As the pressure increases, the lattice strain in the *ab* plane increases which causes a sudden shift in the stacking of alternating MnO layers resulting in a rhombohedral supercell. The volume collapse is thus a consequence of the MnO$_5$ trimer units no longer being stacked perfectly on top of each other which results in a more dense packing. This change occurs at a ratio of $c/a \sim 1.90$, and since the other members of the hexagonal rare-earth manganites show the same compressible behavior of the principle axes, it suggests that a similar response should be expected.

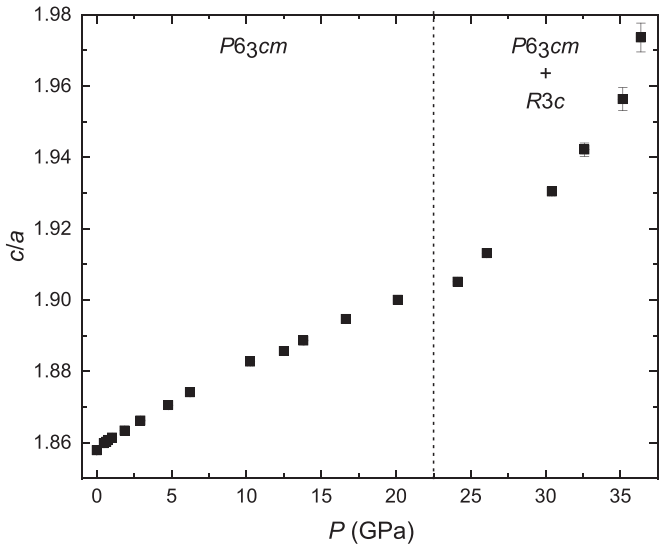

FIG. 6. Cell parameter c/a ratio as a function of pressure of the ambient $P6_3cm$ phase.

Previous pressure studies have reported a pressure-induced phase transition from the hexagonal to the orthorhombic polymorph at 22 GPa for Y(Lu)MnO$_3$ and LuMnO$_3$ by Gao *et al.* [23] (PXRD), 10 GPa for Ho$_{0.8}$Dy$_{0.2}$MnO$_3$ by Feng *et al.* [21] (Raman), 20 GPa for ErMnO$_3$ by Lin *et al.* [24] (PXRD), and 10 GPa for TmMnO$_3$ by Wang *et al.* [22] (PXRD). A summary of observed transitions is also listed in Table I. Common for the PXRD compression studies is the observation of two low-intensity reflections assigned to the orthorhombic structure corresponding to the (111) and (022)/(211) lattice planes accompanied with significant sample strain. While the transition between the hexagonal and orthorhombic polymorph is possible using a combination of high pressure and high temperature [26–28], it seems unlikely this conversion is possible using pressure alone. The two structures are vastly different, with Mn changing coordination number from 5 to 6 and Ho from 7 to 8, and a complete rearrangement of the atoms is necessary to form the three-dimensional octahedral network characteristic of the perovskite structure. Pressure alone is very unlikely to provide the necessary thermal motion for the breaking of bonds and long-range migration of atoms. Common for the mentioned studies is the use of either a 4:1 methanol-ethanol (or 15:3:1 methanol-ethanol-water) mixture or silicone oil as pressure medium. 4:1 methanol-ethanol remains hydrostatic up to ~10.5 GPa where it undergoes a glass transition which can introduce sudden strain-related artifacts due to this sudden change in the pressure medium. Silicone oil has a similar, but more complicated, behavior compared to methanol-ethanol with comparable pressure standard deviations of $\sigma_P \geqslant 2$ GPa at 20 GPa [54]. A more recent study on (Lu)YMnO$_3$ by Jabarov *et al.* [25] observed no phase transitions up to 30 GPa using both PXRD and Raman, in contradiction with the observation made by Gao *et al.* [23] on the same two compounds, despite using the same pressure medium. We therefore performed a second run on h-HoMnO$_3$ using silicone oil as pressure medium for a better understanding of its effect on the phase transition, and to investigate whether a second transition to the orthorhombic

$Pca2_1$ phase would occur at higher pressures. A waterfall plot of this run can be found in the SM [35]. It can be seen that the sample shows signs of a phase transition at 19 GPa with the appearance of the rhombohedral (104) and (108) reflections (marked by stars). However, these reflections do not grow in intensity and no further changes are observed until 30 GPa where the sample undergoes amorphization. The same sensitivity to nonhydrostatic conditions has likewise been demonstrated in isostructural h-RInO$_3$ (R = Y, Eu, Gd, Dy) [52,53]. For more reliable and comparable results a noble gas should preferably be used. Recently, a trigonal local distortion of the MnO_5 bipyramidal units occurring at the boundary between the high-temperature, nonpolar $P6_3/mmc$ and the polar $P6_3cm$ in YMnO$_3$ has been discovered using neutron total scattering [55]. This distortion lowers the local symmetry to $P3c1/P\bar{3}c1$ resulting in three and five nonequivalent Y and O positions, respectively. The same distortion has previously been found in h-InMnO$_3$ [56] and very recently identified as the high-pressure phase of h-$Lu_{0.6}Sc_{0.4}FeO_3$ using combined Raman and IR spectroscopy on single crystals at 15 GPa [57]. We note the many similarities between the trigonal and the rhombohedral distorted structures reported, but assign space group $R3c$ to the h-HoMnO$_3$ high-pressure phase due to the sluggish nature of the phase transition and the apparent volume collapse which are common signs of a first-order phase transition as well as no reflections violating the rhombohedral setting. Invaluable insight into this charge-disproportionation mechanism could be unveiled using simultaneous pressure and temperature dependent polarized micro-Raman on single-crystal samples as the A_1 ($\sim$684 cm^{-1}) phonon mode in h-RMnO$_3$, corresponding to apical oxygen stretching along the z axis, becomes strongly enhanced with increased filling of the $d_{3z^2-r^2}$ orbital which is unpopulated in Mn(III) in its high-spin state [58]. Since the phase transition occurs at a relatively modest pressure, in-house single-crystal x-ray diffraction experiments under pressure are a route which is currently being explored. It is clear that a systematic high-pressure study of h-RMnO$_3$ (R = Ho–Lu) under proper conditions can be expected to reveal similar interesting behavior.

IV. CONCLUSION

Based on our synchrotron HP-PXRD measurements we have discovered a pressure-induced phase in the multiferroic hexagonal rare-earth manganite family, specifically h-HoMnO$_3$. The high-pressure phase was successfully modeled as a $R3c$ supercell of the ambient $P6_3cm$ structure. Interestingly, this phase is isostructural to oxygen-loaded h-RMnO$_{3+\delta}$ (R = Y, Dy, Ho, Er; $\delta \approx 0.28$). The driving force behind the phase transition is likely the high compressibility of the ab plane compared to the c axis, introducing significant strain in the MnO layers resulting in a sudden translational shift of the trimer positions in the high-pressure phase. In addition, we have demonstrated clear evidence of a direct link between the oxygen-loaded h-RMnO$_{3+\delta}$ systems and the high-pressure response by means of XAS with a pressure-induced charge disproportionation of the form 2Mn(III) $\rightarrow$ Mn(IV) + Mn(II). The oxidative properties of Mn are highly sensitive to the size of R but all members of the family exhibit a large compressibility of the ab plane. We therefore expect a similar behavior for the other members in the family, but onset pressure of charge disproportionation and the following phase transition is expected to increase as the ionic radii of R decrease.

ACKNOWLEDGMENTS

We thank the Danish Agency for Science, Technology, and Innovation for funding the instrument center DanScatt. This research was funded by the Independent Research Fund Denmark (Grant No. 7027-00077A) and VILLUM FONDEN via the Centre of Excellence for Dirac Materials (Grant No. 11744). Portions of this work were performed at GeoSoilEnviroCARS (the University of Chicago, Sector 13), Advanced Photon Source (APS), Argonne National Laboratory. GeoSoilEnviroCARS is supported by the National Science Foundation–Earth Sciences (Grant No. EAR-1634415) and Department of Energy–Geosciences (Grant No. DE-FG02-94ER14466). This research used resources of the Advanced Photon Source, a U.S. Department of Energy (DOE) Office of Science User Facility operated for the DOE Office of Science by Argonne National Laboratory under Contract No. DE-AC02-06CH11357. Use of the COMPRES-GSECARS gas-loading system was supported by COMPRES under NSF Cooperative Agreement No. EAR-1606856 and by GSECARS through NSF Grant No. EAR-1634415 and DOE Grant No. DE-FG02-94ER14466. This research used resources of the Advanced Photon Source, a U.S. Department of Energy (DOE) Office of Science User Facility operated for the DOE Office of Science by Argonne National Laboratory under Contract No. DE-AC02-06CH11357. We acknowledge MAX IV Laboratory for time on the beamline DanMAX under Proposal No. 20200703. Research conducted at MAX IV is supported by the Swedish Research Council under Contract No. 2018-07152, the Swedish Governmental Agency for Innovation Systems under Contract No. 2018-04969, and Formas under Contract No. 2019-02496. DanMAX is funded by the NUFI Grant No. 4059-00009B.

[1] S.-W. Cheong and M. Mostovoy, Multiferroics: A magnetic twist for ferroelectricity, Nat. Mater. **6**, 13 (2007).

[2] H. Sim, J. Oh, J. Jeong, M. D. Le, and J.-G. Park, Hexagonal RMnO$_3$: A model system for two-dimensional triangular lattice antiferromagnets, Acta Crystallogr. B: Struct. Sci. Cryst. Eng. Mater. **72**, 3 (2016).

[3] A. P. Levanyuk and D. G. Sannikov, Improper ferroelectrics, Sov. Phys. Usp. **17**, 199 (1974).

[4] T. Kimura, T. Goto, H. Shintani, K. Ishizaka, T. Arima, and Y. Tokura, Magnetic control of ferroelectric polarization, Nature (London) **426**, 55 (2003).

[5] M. Kenzelmann, A. B. Harris, S. Jonas, C. Broholm, J. Schefer, S. B. Kim, C. L. Zhang, S.-W. Cheong, O. P. Vajk, and J. W. Lynn, Magnetic Inversion Symmetry Breaking and Ferroelectricity in TbMnO$_3$, Phys. Rev. Lett. **95**, 087206 (2005).

[6] S. C. Abrahams, Ferroelectricity and structure in the $YMnO_3$ family, Acta Crystallogr. B: Struct. Sci. **57**, 485 (2001).

[7] W. Koehler, H. Yakel, E. Wollan, and J. Cable, A note on the magnetic structures of rare earth manganese oxides, Phys. Lett. **9**, 93 (1964).

[8] K. Łukaszewicz and J. Karut-Kalicińska, X-ray investigations of the crystal structure and phase transitions of $YMnO_3$, Ferroelectrics **7**, 81 (1974).

[9] C. J. Fennie and K. M. Rabe, Ferroelectric transition in $YMnO_3$ from first principles, Phys. Rev. B **72**, 100103(R) (2005).

[10] B. B. Van Aken, T. T. Palstra, A. Filippetti, and N. A. Spaldin, The origin of ferroelectricity in magnetoelectric $YMnO_3$, Nat. Mater. **3**, 164 (2004).

[11] A. Muñoz, J. A. Alonso, M. J. Martínez-Lope, M. T. Casáis, J. L. Martínez, and M. T. Fernández-Díaz, Evolution of the magnetic structure of hexagonal $HoMnO_3$ from neutron powder diffraction data, Chem. Mater. **13**, 1497 (2001).

[12] Z. J. Huang, Y. Cao, Y. Y. Sun, Y. Y. Xue, and C. W. Chu, Coupling between the ferroelectric and antiferromagnetic orders in $YMnO_3$, Phys. Rev. B **56**, 2623 (1997).

[13] N. Iwata and K. Kohn, Dielectric anomalies at magnetic transitions of hexagonal rare earth manganese oxides $R MnO_3$, J. Phys. Soc. Jpn. **67**, 3318 (1998).

[14] T. Katsufuji, S. Mori, M. Masaki, Y. Moritomo, N. Yamamoto, and H. Takagi, Dielectric and magnetic anomalies and spin frustration in hexagonal $R MnO_3 (R = \mathrm{Y}, \mathrm{Yb}, \text{and } \mathrm{Lu})$, Phys. Rev. B **64**, 104419 (2001).

[15] H. Sugie, N. Iwata, and K. Kohn, Magnetic ordering of rare earth ions and magnetic-electric interaction of hexagonal $R MnO_3$ (R = Ho, Er, Yb, or Lu), J. Phys. Soc. Jpn. **71**, 1558 (2002).

[16] C. dela Cruz, F. Yen, B. Lorenz, Y. Q. Wang, Y. Y. Sun, M. M. Gospodinov, and C. W. Chu, Strong spin-lattice coupling in multiferroic $HoMnO_3$: Thermal expansion anomalies and pressure effect, Phys. Rev. B **71**, 060407(R) (2005).

[17] S. Lee, A. Pirogov, M. Kang, K.-H. Jang, M. Yonemura, T. Kamiyama, S.-W. Cheong, F. Gozzo, N. Shin, H. Kimura, Y. Noda, and J.-G. Park, Giant magneto-elastic coupling in multiferroic hexagonal manganites, Nature (London) **451**, 805 (2008).

[18] J. Park, J.-G. Park, G. S. Jeon, H.-Y. Choi, C. Lee, W. Jo, R. Bewley, K. A. McEwen, and T. G. Perring, Magnetic ordering and spin-liquid state of $YMnO_3$, Phys. Rev. B **68**, 104426 (2003).

[19] J. Kim, X. Wang, F.-T. Huang, Y. Wang, X. Fang, X. Luo, Y. Li, M. Wu, S. Mori, D. Kwok, E. D. Mun, V. S. Zapf, and S.-W. Cheong, Spin Liquid State and Topological Structural Defects in Hexagonal $TbInO_3$, Phys. Rev. X **9**, 031005 (2019).

[20] S. Janas, J. Lass, A.-E. Ţuţueanu, M. L. Haubro, C. Niedermayer, U. Stuhr, G. Xu, D. Prabhakaran, P. P. Deen, S. Holm-Dahlin, and K. Lefmann, Classical Spin Liquid or Extended Critical Range in $h - YMnO_3$? Phys. Rev. Lett. **126**, 107203 (2021).

[21] S. M. Feng, L. J. Wang, J. L. Zhu, F. Y. Li, R. C. Yu, C. Q. Jin, X. H. Wang, and L. T. Li, Pressure-induced phase transition in $Ho_{0.8}Dy_{0.2}MnO_3$ multiferroic compound, J. Appl. Phys. **103**, 026102 (2008).

[22] L. J. Wang, S. M. Feng, J. L. Zhu, Q. Q. Liu, Y. C. Li, X. D. Li, J. Liu, and C. Q. Jin, Structure transition of multiferroic hexagonal $TmMnO_3$ compound under high pressure, High Press. Res. **30**, 258 (2010).

[23] P. Gao, Z. Chen, T. A. Tyson, T. Wu, K. H. Ahn, Z. Liu, R. Tappero, S. B. Kim, and S.-W. Cheong, High-pressure structural stability of multiferroic hexagonal $R MnO_3$ (R = Y, Ho, Lu), Phys. Rev. B **83**, 224113 (2011).

[24] C. Lin, J. Liu, X. Li, Y. Li, S. Chu, L. Xiong, and R. Li, Phase transformation in hexagonal $ErMnO_3$ under high pressure, J. Appl. Phys. **112**, 113512 (2012).

[25] S. H. Jabarov, N. T. Dang, S. E. Kichanov, D. P. Kozlenko, L. S. Dubrovinsky, J.-G. Park, S. Lee, A. I. Mammadov, R. Z. Mehdiyeva, B. N. Savenko, N. X. Nghia, L. H. Khiem, N. T. T. Lieu, and L. T. P. Thao, Crystal structure and vibrational spectra of hexagonal manganites $YMnO_3$ and $LuMnO_3$ under high pressure, Mater. Res. Express **6**, 086110 (2019).

[26] A. Waintal, J. Capponi, E. Bertaut, M. Contré, and D. François, Transformation sous haute pression de la forme ferroelectrique de $HoMnO_3$ en une forme perovskite paraelectrique, Solid State Commun. **4**, 125 (1966).

[27] Y. H. Huang, H. Fjellvåg, M. Karppinen, B. C. Hauback, H. Yamauchi, and J. B. Goodenough, Crystal and magnetic structure of the orthorhombic perovskite $YMnO_3$, Chem. Mater. **18**, 2130 (2006).

[28] K. Uusi-Esko, J. Malm, N. Imamura, H. Yamauchi, and M. Karppinen, Characterization of $R MnO_3$ (R=Sc, Y, Dy-Lu): High-pressure synthesized metastable perovskites and their hexagonal precursor phases, Mater. Chem. Phys. **112**, 1029 (2008).

[29] G. Shen, V. B. Prakapenka, P. J. Eng, M. L. Rivers, and S. R. Sutton, Facilities for high-pressure research with the diamond anvil cell at GSECARS, J. Synchrotron Radiat. **12**, 642 (2005).

[30] M. Rivers, V. B. Prakapenka, A. Kubo, C. Pullins, C. M. Holl, and S. D. Jacobsen, The COMPRES/GSECARS gas-loading system for diamond anvil cells at the Advanced Photon Source, High Press. Res. **28**, 273 (2008).

[31] C. Prescher and V. B. Prakapenka, DIOPTAS: A program for reduction of two-dimensional x-ray diffraction data and data exploration, High Press. Res. **35**, 223 (2015).

[32] J. Rodríguez-Carvajal, Recent advances in magnetic structure determination by neutron powder diffraction, Phys. B: Condens. Matter **192**, 55 (1993).

[33] R. J. Angel, M. Alvaro, and J. Gonzalez-Platas, EosFit7c and a Fortran module (library) for equation of state calculations, Z. Kristallogr. - Cryst. Mater. **229**, 405 (2014).

[34] K. Momma and F. Izumi, *VESTA3* for three-dimensional visualization of crystal, volumetric and morphology data, J. Appl. Crystallogr. **44**, 1272 (2011).

[35] See Supplemental Material at http://link.aps.org/supplemental/10.1103/PhysRevB.107.134115 for structural refinement parameters, HP-PXRD waterfall plot (PTM silicone oil), and the evolution of the Ho L_3 edge with pressure.

[36] F. Baudelet, Q. Kong, L. Nataf, J. D. Cafun, A. Congeduti, A. Monza, S. Chagnot, and J. P. Itié, ODE: A new beam line for high-pressure XAS and XMCD studies at SOLEIL, High Press. Res. **31**, 136 (2011).

[37] A. Dewaele, M. Torrent, P. Loubeyre, and M. Mezouar, Compression curves of transition metals in the Mbar range: Experiments and projector augmented-wave calculations, Phys. Rev. B **78**, 104102 (2008).

[38] B. Ravel and M. Newville, *ATHENA*, *ARTEMIS*, *HEPHAESTUS*: Data analysis for x-ray absorption spectroscopy using *IFEFFIT*, J. Synchrotron Radiat. **12**, 537 (2005).

[39] S. Remsen, B. Dabrowski, O. Chmaissem, J. Mais, and A. Szewczyk, Synthesis and oxygen content dependent properties of hexagonal $DyMnO_{3+\delta}$, J. Solid State Chem. **184**, 2306 (2011).

[40] C. Abughayada, B. Dabrowski, S. Kolesnik, D. E. Brown, and O. Chmaissem, Characterization of oxygen storage and structural properties of oxygen-loaded hexagonal $RMnO_{3+\delta}$ (R = Ho, Er, and Y), Chem. Mater. **27**, 6259 (2015).

[41] K. Świerczek, A. Klimkowicz, K. Nishihara, S. Kobayashi, A. Takasaki, M. Alanizy, S. Kolesnik, B. Dabrowski, S. Seong, and J. Kang, Oxygen storage properties of hexagonal $HoMnO_{3+\delta}$, Phys. Chem. Chem. Phys. **19**, 19243 (2017).

[42] S. Remsen and B. Dabrowski, Synthesis and oxygen storage capacities of hexagonal $Dy_{1-x}Y_xMnO_{3+\delta}$, Chem. Mater. **23**, 3818 (2011).

[43] T. Asaka, K. Nemoto, K. Kimoto, T. Arima, and Y. Matsui, Crystallographic superstructure of Ti-doped hexagonal $YMnO_3$, Phys. Rev. B **71**, 014114 (2005).

[44] I. Levin, V. Krayzman, T. Vanderah, M. Tomczyk, H. Wu, M. Tucker, H. Playford, J. Woicik, C. Dennis, and P. Vilarinho, Oxygen-storage behavior and local structure in Ti-substituted $YMnO_3$, J. Solid State Chem. **246**, 29 (2017).

[45] Y. Aikawa, T. Katsufuji, T. Arima, and K. Kato, Effect of Mn trimerization on the magnetic and dielectric properties of hexagonal $YMnO_3$, Phys. Rev. B **71**, 184418 (2005).

[46] F. Farges, *Ab initio* and experimental pre-edge investigations of the Mn *K*-edge XANES in oxide-type materials, Phys. Rev. B **71**, 155109 (2005).

[47] D. P. Kozlenko, S. E. Kichanov, E. V. Lukin, S. Lee, J.-G. Park, and B. N. Savenko, Spin fluctuations and structural modifications in frustrated multiferroics $RMnO_3$ (R =Y, Lu) at high pressure, High Press. Res. **30**, 252 (2010).

[48] D. P. Kozlenko, I. Mirebeau, J.-G. Park, I. N. Goncharenko, S. Lee, J. Park, and B. N. Savenko, High-pressure-induced spin-liquid phase of multiferroic $YMnO_3$, Phys. Rev. B **78**, 054401 (2008).

[49] T. Katsufuji, M. Masaki, A. Machida, M. Moritomo, K. Kato, E. Nishibori, M. Takata, M. Sakata, K. Ohoyama, K. Kitazawa, and H. Takagi, Crystal structure and magnetic properties of hexagonal $RMnO_3$(R = Y, Lu, and Sc) and the effect of doping, Phys. Rev. B **66**, 134434 (2002).

[50] R. D. Shannon, Revised effective ionic radii and systematic studies of interatomic distances in halides and chalcogenides, Acta Crystallogr., Sect. A **32**, 751 (1976).

[51] Y. Jia, Crystal radii and effective ionic radii of the rare earth ions, J. Solid State Chem. **95**, 184 (1991).

[52] A. Dwivedi, H. K. Poswal, R. Shukla, S. Velaga, B. D. Sahoo, V. Grover, and M. N. Deo, High pressure structural investigations on hexagonal $YInO_3$, High Press. Res. **39**, 17 (2019).

[53] C. Lin, J. Liu, Y. Li, X. Li, and R. Li, Pressure-induced structural and vibrational evolution in ferroelectric $RInO_3$ (R = Eu, Gd, Dy), Solid State Commun. **173**, 51 (2013).

[54] S. Klotz, J.-C. Chervin, P. Munsch, and G. L. Marchand, Hydrostatic limits of 11 pressure transmitting media, J. Phys. D **42**, 075413 (2009).

[55] S. H. Skjærvø, Q. N. Meier, M. Feygenson, N. A. Spaldin, S. J. L. Billinge, E. S. Bozin, and S. M. Selbach, Unconventional Continuous Structural Disorder at the Order-Disorder Phase Transition in the Hexagonal Manganites, Phys. Rev. X **9**, 031001 (2019).

[56] F.-T. Huang, X. Wang, S. M. Griffin, Y. Kumagai, O. Gindele, M.-W. Chu, Y. Horibe, N. A. Spaldin, and S.-W. Cheong, Duality of Topological Defects in Hexagonal Manganites, Phys. Rev. Lett. **113**, 267602 (2014).

[57] K. A. Smith, S. P. Ramkumar, N. C. Harms, A. J. Clune, S.-W. Cheong, Z. Liu, E. A. Nowadnick, and J. L. Musfeldt, Pressure-induced phase transition and phonon softening in h-$Lu_{0.6}Sc_{0.4}FeO_3$, Phys. Rev. B **104**, 094109 (2021).

[58] J. Vermette, S. Jandl, and M. M. Gospodinov, Raman study of spin–phonon coupling in $ErMnO_3$, J. Phys.: Condens. Matter **20**, 425219 (2008).